In situ transcriptional profile of a germinal center plasmablastic burst hints at an unfavorable Diffuse Large B-cell Lymphoma subset.

Vincenzo L'Imperio[1]*, Gaia Morello[2]*, Valeria Cancila[2], Giorgio Bertolazzi[2], Saveria Mazzara[3], Beatrice Belmonte[2], Piera Balzarini[4], Lilia Corral[5], Arianna Di Napoli[6], Fabio Facchetti[7], Fabio Pagni[1]*, Claudio Tripodo[2,8]*

[1] Department of Medicine and Surgery, University of Milano-Bicocca, Pathology, San Gerardo Hospital, Via G.B. Pergolesi 33, Monza, Italy.
[2] Tumor Immunology Unit, Department of Sciences for Health Promotion and Mother-Child Care "G. D'Alessandro", University of Palermo, Palermo, Italy.
[3] Division of Diagnostic Haematopathology, European Institute of Oncology, Milan, Italy.
[4] Department of Molecular and Translational Medicine, University of Brescia, Piazzale Spedali Civili 1, 25123, Brescia, Italy.
[5] Centro Ricerca Tettamanti, Pediatric Clinic, University of Milan Bicocca, San Gerardo Hospital/Fondazione MBBM, Monza, Italy.
[6] Pathology Unit, Sapienza University of Rome, Sant'Andrea Hospital, Rome, Italy.
[7] Pathology Unit, University of Brescia, Brescia, Italy.
[8] Tumor and Microenvironment Histopathology Unit, IFOM, the FIRC Institute of Molecular Oncology, Milan, Italy.

* These Authors equally contributed

Correspondence:

Prof. Claudio Tripodo, Tumor Immunology Unit, University of Palermo, Corso Tukory 211, 90134, Palermo. Phone +3909123896211. Email: claudio.tripodo@unipa.it

Abstract

The germinal center (GC) reaction results in the selection of B-cells acquiring effector Ig secreting ability by progressing towards plasmablastic differentiation. This transition is associated with exclusion from the GC microenvironment. The aberrant expansion of plasmablastic elements within the GC fringes configures an atypical condition, the biological characteristics of which have not been defined yet. We investigated the *in situ* immunophenotypical and transcriptional characteristics of a non-clonal germinotropic expansion of plasmablastic elements (GEx) occurring in the tonsil of a young patient. Compared to neighboring GC and peri-follicular regions, the GEx showed a distinctive signature featuring key regulators of plasmacytic differentiation, cytokine signaling, and cell metabolism. The GEx signature was tested in the setting of diffuse large B-cell lymphoma (DLBCL) as a prototypical model of lymphomagenesis encompassing transformation at different stages of GC and post-GC functional differentiation. The signature outlined DLBCL clusters with different overall survival, highlighting the negative prognostic significance of the overexpression of hallmark genes of this peculiar condition.

Running title: Spatial profiling of a germinotropic plasmablastic expansion

Keywords: digital spatial profiling, germinal center, plasmablast, diffuse large B-cell lymphoma.

57 **Introduction**

58 Within secondary lymphoid organs immune cells display topographic compartmentalization
59 underlying functional commitment towards different stages of immune response induction and
60 regulation. In lymphoid follicles, germinal centers (GCs) represent a complex specialized
61 microenvironment sustaining B-cell proliferative bursts underlying somatic hypermutation and
62 class-switch recombination of immunoglobulin (Ig) genes, communication with T cell subsets
63 with helping function (Tfh), and interplay with specialized mesenchymal scaffolds (i.e. FDCs)
64 (1). These events play through the dynamical iteration of elements between the dark (DZ),
65 intermediate and light (LZ) zones of the GC (2), eventually resulting in the differentiation and
66 displacement from the GC of cells acquiring effector capabilities through the synthesis and
67 secretion of Igs (i.e. plasmablasts and plasma cells) (3). Alterations in the topographic
68 compartmentalization of GC and extra-GC populations in lymphoid tissues are commonly
69 observed in the setting of lymphoproliferative diseases, where the accumulation of cells with
70 morphological or immunophenotypical features conflicting with their topographic localization
71 represents a hallmark of histopathological analyses. This assumption reached its highest
72 expression with the introduction of a diffuse large B cell lymphoma (DLBCL) prognostic sub-
73 classification based on the presumed cell-of-origin (COO), as determined by gene expression
74 profiling (GEP) (4-6).

75 We have investigated here an atypical germinotropic expansion of non-clonal, light-chain
76 restricted B cells with plasmablastic features confined to a single enlarged GC structure in the
77 tonsil of a young patient, through in situ immunolocalization analyses and high throughput
78 digital spatial profiling. Comparing the features of the atypical germinotropic expansion (GEx)
79 with those of topographically preserved DZ, LZ and peri-follicular (PERI) regions of interest
80 (ROIs) we identified a unique transcriptomic profile of the GEx ROIs featuring the

overexpression of transcripts involved in plasmacytoid differentiation, cytokine signaling, and cell metabolism.

To probe the reflection of the identified transcriptional signature in a setting of B-cell lymphomatous transformation embracing the full spectrum of GC- and post-GC differentiation, the discriminative 20 genes were used to cluster a large cohort of diffuse large B-cell lymphoma (DLBCL) transcriptomic data. The GEx signature highlighted two clusters with different overall survival in DLBCL, where cases with the highest expression of GEx hallmark genes were characterized by poorer prognosis.

Materials and methods

Clinical setting

This study started from the incidental finding of the reactive germinotropic plasmablastic expansion described in the Results section, in the tonsil of a young patient who underwent tonsillectomy for clinical hypertrophy. Sample was obtained and handled according to the Declaration of Helsinki. Informed consent for surgery and histopathological studies was obtained from the legal representatives. The case was included in the study 05/2018 approved by the University of Palermo Institutional Review Board.

Histological, immunohistochemical and molecular analyses

Tonsillar tissue has been formalin-fixed and paraffin-embedded (FFPE) and 3 μm thick sections have been stained with hematoxylin and eosin (H&E). IHC has been performed at the Pathology Department of ASST Monza, San Gerardo Hospital, Monza, Italy using a Dako Omnis platform (Dako, Denmark) using antibodies directed against CD20 (L26), CD3 (Polyclonal), Bcl2 (124), Bcl6 (PG-B6p), CD21, ki-67 (Mib-1), MUM1, CD10, CD30 (Ber-H2), CD138 (Mi15), HHV8 (13B10), kappa and lambda light chains. Double

106 immunohistochemistry has been performed for MUM1 and CD10 using 3-3'-diaminobenzidine
107 (DAB) and 3-amino-9-ethylcarbazole (AEC) as chromogens, respectively. In situ fluorescence
108 hybridization (FISH) study has been performed using a IRF4/DUSP22 (6p25) Break Apart kit
109 (Kreatech, Leica Biosystem, Germany) at the Pathology Department of Spedali Riuniti di
110 Brescia. Quantitative evaluation of immunophenotypical markers was performed by applying
111 the HALO image analysis software (v3.2.1851.229, Indica Labs) to regions selected on whole
112 slide digital scans acquired using an Aperio CS2 slide scanner with the ImageScope software
113 (v12.3.28013, Leica Biosystems, Germany).
114 Quantitative polymerase chain reaction (Q-PCR) to detect clonal immunoglobulin genes
115 rearrangement was performed after laser microdissection on H&E-stained slides, using an
116 LMD6 platform (Leica Microsystems, Germany).
117 *Digital spatial profiling*
118 The transcriptional landscape of 15 different spatially-resolved regions of interests (ROIs) of
119 the tonsil (5 peri/inter-follicular ROIs, 5 DZ and 5 LZ ROIs from morphologically normal
120 follicles) and 9 ROIs from the GEx was determined by Digital Spatial Profiling on slides
121 stained with CD271/NGFR (as an FDC marker to highlight the LZ) and CD20 (as a B-cell
122 marker). The 24 selected and segmented ROIs were profiled using a GeoMx Digital Spatial
123 Profiler (DSP) (NanoString, Seattle WA) as previously described (7), applying the Cancer
124 Transcriptome Atlas panel (https://www.nanostring.com/products/geomx-digital-spatial-
125 profiler/geomx-rna-assays/geomx-cancer-transcriptome-atlas/) (Supplementary Table 1).
126 *Bioinformatic Data Analysis*
127 After quality check step, raw counts were normalized against the 75th percentile of signal from
128 their own ROI and normalized data were used to perform PCA using FactoMine R package.
129 For hierarchical clustering analysis of the ROIs the Euclidean distance metric across samples

130 was considered and complete aggregation method was used for building tree within the R
131 package hclust.
132 Differential expression analyses were carried out by applying the moderated t-test using the
133 limma package (8); pairwise comparisons between GEx and DZ/LZ/Peri ROIs were
134 considered. Upregulated/downregulated genes were selected for subsequent analysis if their
135 expression values were found to exceed the threshold of 0.05 FWER (Bonferroni correction).
136 The spatial GEx signature was assessed in the following GEO datasets: GSE32918 (9) and
137 GSE117556 (10). First, samples with a low Pearson correlation coefficient with other samples
138 in the space of all genes for each separately dataset were removed as proposed by Kotlov et
139 al.(28). Probe sets were annotated using the annotation files from IlluminaHumanv4.db and
140 illumina Humanv3.db . When multiple probes were associated to the same we collapsed to the
141 average value. Next, the two transcriptomic datasets were combined and a quantile
142 normalization was performed using preprocess Core package. Furthermore, possible batch
143 effects were corrected with limma package and a PCA was considered to verify the effective
144 removal of the batch effects.

145 The clinical information for rGSE32918 cohort (9) was downloaded from GEO repository
146 while, forGSE117556 cohort was retrieved from the supplementary material of Sha et al (10).

147 After performing z-score, unsupervised hierarchical clustering analysis based on the GEx
148 signature was applied to identify potential discriminative clusters based on Ward.D2 method
149 on the Euclidean distance of z-score expression. Silhouette and the elbow methods, from the
150 factoextra R package were employed to choose the optimal number of clusters. Differences in
151 the total GEx signature expression inside clusters were evaluated using a Kolmogorov-Smirnov
152 test on ECDFs. The Cox model has been fitted to estimate the relative risk of death between
153 clusters. Before calculating the log-rank test and fitting the Cox model, the cox.pzh test has

154 been used to test the proportional hazard assumption. In order to directly evaluate the
155 association between patient survival time and expression of the GEx signature, we assessed a
156 quantile strategy to split patients into four groups. To analyze the prognostic value of GEx
157 signature, merged cohort was dichotomized into higher (GEx expression is greater than the 75th
158 quantile) and lower groups (GEx expression is lower than the 25th quantile) whereas patients
159 with the GEx expression between the two extremes were excluded from the survival analysis.
160 Difference in patient characteristics was analyzed with the Fisher's exact test.

161 All statistical analyses were performed using R statistical software (v4.0.2, http://www.R-
162 project.org).

163 *Data Availability*

164 Normalized gene expression data generated in the Digital Spatial Profiling experiment are
165 available in Supplementary Table 1
166
167
168 **Results**
169 *Pathology of the tonsil*
170 Histopathological analysis of the left tonsil from a young patient with clinical bilateral
171 hypertrophy revealed, in a background of lymphoid follicles with hyperplastic features and
172 preserved GC DZ, LZ and mantles, an isolated abnormal follicle with flattened mantle zone,
173 an enlarged GC, without evident DZ/LZ polarization, preservation of rare tingible body
174 macrophages, and populated by a predominance of monomorphic plasmacytoid cells with
175 immature morphology (Figure 1A). Quantitative immunophenotypical characterization of
176 reactive follicular and peri-follicular regions and of the atypical germinotropic plasmablasts
177 (GEx), highlighted conspicuous differences in the immune profile (Figure 1B-C). The reactive

178 preserved DZ and LZ of GCs were characterized by B cells with strong CD20 expression, dense
179 Ki-67 immunoreactivity (higher in the DZ), negativity for IRF4, except for scattered cells in a
180 background of CD10-expressing cells, Bcl-2 negativity, slight T-cell infiltration (denser in the
181 LZ), and no evidence of light chain restriction (Figure 1B-C). At contrast, the composition of
182 the GEx displayed a CD20+ B cell phenotype, high Ki-67+ proliferative fraction, diffuse IRF4
183 positivity with IRF4+ cells co-expressing CD10, negativity for Bcl-2, and
184 immunophenotypical restriction for lambda light chain (Figure 1B-C). Most of the cells
185 populating the GEx also expressed CD138 in the absence of CD30, indicating partial
186 acquisition of a plasmablastic phenotype. Immunoistochemistry for HHV8 and *in situ*
187 hybridization for EBER (EBV) proved negative (Supplementary Figure 1). On the basis of the
188 GEx lambda light chain restriction, analysis of the Ig light and heavy genes rearrangement was
189 performed on DNA extracted by laser microdissection of the GEx, which revealed a polyclonal
190 profile (Supplementary Figure 2). The strong and diffuse immunoreactivity of IRF4 and the
191 co-occurrence of IRF4/CD10 double-expressing elements prompted the analysis of *IRF4* gene
192 rearrangement by fluorescence in situ hybridization (FISH), which did not reveal any
193 abnormality (Supplementary Figure 3), allowing to exclude an IRF4-rearranged lymphoma.
194
195 *Digital Spatial Profiling of the GEx regions reveals a distinctive profile*
196 The molecular profiles of non-malignant GC compartments can be exploited to probe GC
197 microenvironment imprints in B-cell lymphomas with different degree of relationship with GC
198 subpopulations, such as DLBCL, in which the COO has shown prognostic significance in the
199 setting of standard chemo-immunotherapy regimens (7). We had the opportunity to probe the
200 in situ transcriptional profile of a yet unexplored atypical configuration of a GC proliferative
201 burst. Through the Nanostring GeoMx technology, the expression of 1824 genes from key
202 cancer-associated transcriptional programs (Supplementary Table 1) was determined on 5 DZ,

203 5 LZ and 5 PERI ROIs selected from morphologically/phenotypically preserved
204 follicles/perifollicular areas, and on 9 GEx ROIs. We then asked whether GEx ROIs could be
205 defined by a specific gene signature; to this aim, principal component analysis (PCA) and
206 unsupervised hierarchical clustering were investigated. PCA revealed that ROIs segregated
207 according to their spatial classification, with PERI regions showing neatly separated profiles
208 from GC ROIs including DZ, LZ and GEx and GEx ROIs clustered together with other GC
209 regions, showing some degree of intermixing with LZ ROIs (Figure 2A). Consistently,
210 clustering analysis confirmed the same degree of relationship between the different ROIs
211 (Figure 2B). mRNA expression of the transcripts relative to the IHC markers evaluated for
212 quantitative immunopehnotypical analyses showed consistency with the protein expression
213 pattern (Supplementary Figure 4). Pairwise differential expression analysis performed on the
214 different ROIs allowed to identify candidate genes reflecting the distinctive profiles between
215 the GEx ROIs in comparison with DZ LZ and PERI ROIs (Figure 2C-F). Among the 20 genes,
216 17 were significantly upregulated in GEx ROIs, while 3 were downmodulated (Figure 2C-F).
217 GEx hallmark genes included, along with the plasma cell differentiation markers *PRDM1*,
218 *IRF4*, *TNFRSF17* (BCMA) and *CD9*, genes involved in 2-oxoglutarate metabolism (*GOT2*,
219 *IDH2)*, in IL17 pathway (*IL17RB, HSP90B1*) and cytokine signaling (*RASAL1*, *LTB*), in PI3K-
220 Akt pathway (*SGK1, BCL2L1*), in lymphocyte activation (*ADA*, *SCL7A5, FCRL2*) and cell
221 surface regulation of immune activation (*CD24, LILRB1*), in cell adhesion (*ANKRD28*) and
222 response to abiotic (i.e. osmotic) stress (*SLK1*). Moreover, the long non-coding RNA *FAM30*
223 was also listed among the GEx hallmarks.
224
225 *The GEx signature outlines a subset of DLBCL with unfavorable prognosis*
226 To investigate whether the transcriptional hallmarks identified in the GEx ROIs could be traced
227 in the heterogeneous spectrum of B-cell malignant transformation recapitulated by DLBCL,

228 we applied the GEx gene signature to a harmonized dataset of 1147 DLBCL cases relative to
229 GSE32918 (9) and GSE117556 (10). Based on the expression of the GEx signature (19 protein-
230 coding genes), DLBCL clustered into two main groups (Figure 3A), with the cluster 1
231 characterized by significantly different enrichment in ABC cases (Fisher exact test p-value <
232 10e-10) and significantly worst overall survival (Figure 3A-B, relative risk (RR) = 1.61, p-val
233 < 0.001). Since 17 out of the 20 GEx differential genes were overexpressed as compared with
234 DZ, LZ, and PERI ROIs, we comparatively analyzed DLBCL cases expressing high or low
235 levels of the GEx overexpressed genes focusing on the Q1 and Q4 quartiles of their cumulative
236 expression (Figure 3C). DLBCL cases characterized by highest (Q4) cumulative expression of
237 the GEx genes had a significantly poorer OS as compared with cases characterized by the
238 lowest expression (Q1) (Figure 3C, RR = 1.63, p-value = 0.002). The negative prognostic value
239 of the GEx overexpressed genes was significant also when ABC DLBCL cases only were
240 considered (Figure 3D, RR = 1.79, p-val = 0.04), while it was lost in the GCB DLBCL subset
241 (Figure 3E, RR = 1.22, p-val = 0.37), suggesting that the genes positively characterizing GEx
242 ROIs underlie a specific biology related with the ABC COO, known to be enriched in clones
243 undergoing plasmablastic/plasmacytic commitment.
244
245 **Discussion**
246 Plasma cells (PCs) represent the final step of the functional differentiation process of the B
247 lymphocyte, through the transition in short-living highly proliferative plasmablasts. The
248 transition of B cells undergoing selection and refinement of their IG receptor in the GC reaction
249 towards effectors capable of Ig secretion implies the acquisition of plasmablastic/plasmacytoid
250 features within the GC microenvironment. The spatial localization of these functional and
251 phenotypical intermediates is still poorly characterized and depends on the dynamical
252 modulation of chemotactic receptor/ligand axes interweaving with BCR-controlled programs

253 (11). Proliferating cells with plasmablastic/plasmacytoid features accumulating within the GC
254 therefore represents an element of atypia even in the setting of non-clonal events, and little is
255 known about the *molecular signature* characterizing their transient state (12). In this report we
256 phenotypically and transcriptionally characterized an immunoglobulin light chain restricted
257 non-clonal atypical germinotropic expansion of plasmablastic cells, investigating differential
258 features emerging from the comparison with neighboring GC and extra-GC regions. The GEx
259 ROIs were characterized by the unique co-occurrence of IRF4 and CD10 expression, which
260 highlighted a transitory state engendered by IRF4 control of GC exit (13) and CD10
261 ectopeptidase retention that can be observed in DLBCL with plasmablastic differentiation (14).
262 On digital spatial profiling, a set of 20 genes were found differentially expressed in GEx ROIs
263 as compared with neighboring DZ, LZ and PERI ROIs. The discriminating signature resulted
264 positively enriched in the key transcription factors driving plasma cell differentiation IRF4 and
265 PRDM1, and included the B-cell differentiation receptor BCMA involved in the transduction
266 of trophic signals from APRIL and BAFF tumor necrosis factor superfamily ligands (15). Such
267 molecular features supportive of a plasmablastic phenotype were also supported by the
268 downregulation of CD24, a signal transducer negatively modulated in response to BCR
269 activation and along plasmablastic transition (16). The GC localization of the plasmablastic
270 expansion found resonance in the overexpression of CD9. The tetraspanin CD9 has been
271 reported to mark a subset of B cells in the human GC characterized by plasmablastic
272 differentiation and Blimp1 (*PRDM1*) expression (17). These CD9+ GC B cells more efficiently
273 give rise to CD20-CD38+ plasmablasts as compared with their CD9- counterpart. Moreover,
274 in the murine setting, the efficient plasmablastic/plasmacytic differentiation of CD9+ B cells
275 is shared by non-GC B-cells endowed with prompt commitment to Ig-secreting effectors, such
276 as B1 B cells and marginal zone B-cells subsets (18). By applying the GEx differentially
277 expressed genes signature to DLBCL we aimed at investigating whether the atypical status of

278 non-clonal germinotropic plasmablastic expansion could be represented in the transcriptional
279 signature of a subset of DLBCL of either ABC or GCB COO. Previous reports described a
280 subset of ABC-DLBCL expressing *PRDM1*/BLIMP1 and demonstrated that loss of function
281 of this antigen is harbinger of a poor prognosis (19). Expression of IRF4/MUM1 is routinely
282 employed in the diagnostic setting for the distinction of non-GC subtypes based on
283 immunohistochemical algorithms (20). Moreover, specific subtypes of large B-cell lymphomas
284 characterized by IRF4 rearrangement have been recently described and recognized as
285 independent entities in the most recent WHO classification (21). We report additional
286 molecular markers potentially associated with plasmablastic commitment in the GC, including
287 the receptor of IL17B/IL25 IL17RB, the overexpression of which marks lymphoplasmacytic
288 lymphomas with mutant $MYD88^{L265P}$ and $CXCR4^{WT}$ (22). In the GC setting, IL17B/IL25
289 signaling could enforce NF-κB activity (23) through TRAF6, which cooperation with CD40
290 signaling is required for B-cell affinity maturation and plasma cell differentiation (24). From
291 the genes positively and negatively characterizing GEx ROIs, no relevant clues emerge about
292 the mechanisms leading to the atypical GC retention and expansion of the plasmablastic
293 elements. Under normal conditions, the suppression of Bach2 and Pax5 transcripts, along with
294 the down-regulation of Bcl-6, IRF8 and PU-1 and the activation of BLIMP1 and MUM1/IRF4,
295 drive the development of PCs resulting from the GC reaction (1). Once their effector/memory
296 fate is established, B cells escape from the GCs through the suppression of the BCL-6-induced
297 "confinement factor" S1PR2 and the expression of pro-migratory receptors that are likely to be
298 involved in GC exit, such as EBI2 and S1PR1 (25). The downmodulation of lymphotoxin beta
299 transcript emerging from the GEx ROIs profiling can imply an impaired activation of the FDC
300 meshwork by resident elements (26) which would in turn impact on the maintenance of a
301 functional GC microenvironment licensing atypical plasmablastic expansion within the GC
302 contexture. Indeed, some cases of abrupt/florid follicular hyperplasia have been described in

303 which activated B cells are mainly localized in the GCs, partly twisting the normal follicular
304 architecture and even showing immunohistochemical light chain (oligoclonal) restriction,
305 leading to diagnostic concern for neoplasia (27). The evidence of a negative prognostic
306 significance of the GEx hallmark genes in a large harmonized dataset, which proved to be
307 significant in ABC but not in GCB cases, suggests that within the heterogeneous ABC COO,
308 in which specific genetic subgroups are enriched, GC-related proliferations of plasmablastic
309 elements could be represented. Genetic studies in such cases in which a dyscrasia between
310 cyto-architectural, phenotypical and topographic profile of a B-cell expansion with
311 plasmablastic/plasmacytic features may help in finding a link with specific genetic subsets of
312 DLBCL (28) and reconcile an ABC-COO with GC-like microenvironment features (29).
313
314

315 **Acknowledgements**

316 The Authors wish to acknowledge Prof. Maurilio Ponzoni for helpful discussion. This study
317 has been supported by the Italian Foundation for Cancer Research (AIRC) through the IG-2018
318 22145 Investigator Grant to C.T.; 5x1000 22759 Grant to C.T.; and by the Italian Ministry of
319 Education, University and Research (MIUR) grant 2017K7FSYB to C.T.

320

321

322

REFERENCES

1. De Silva NS, Klein U. Dynamics of B cells in germinal centres. Nat Rev Immunol. 2015 Mar;15(3):137-48. doi: 10.1038/nri3804. Epub 2015 Feb 6. PMID: 25656706; PMCID: PMC4399774.

2. Allen CD, Okada T, Cyster JG. Germinal-center organization and cellular dynamics. Immunity. 2007 Aug;27(2):190-202. doi: 10.1016/j.immuni.2007.07.009. PMID: 17723214; PMCID: PMC2242846.

3. Yam-Puc JC, Zhang L, Maqueda-Alfaro RA, Garcia-Ibanez L, Zhang Y, Davies J et al. Enhanced BCR signaling inflicts early plasmablast and germinal center B cell death. iScience. 2021 Jan 7;24(2):102038. doi: 10.1016/j.isci.2021.102038. PMID: 33532715; PMCID: PMC7822941.

4. Alizadeh AA, Eisen MB, Davis RE, Ma C, Lossos IS, Rosenwald A et al. Distinct types of diffuse large B-cell lymphoma identified by gene expression profiling. Nature. 2000 Feb 3;403(6769):503-11. doi: 10.1038/35000501. PMID: 10676951.

5. Chapuy B, Stewart C, Dunford AJ, Kim J, Kamburov A, Redd RA et al. Molecular subtypes of diffuse large B cell lymphoma are associated with distinct pathogenic mechanisms and outcomes. Nat Med. 2018 May;24(5):679-690. doi: 10.1038/s41591-018-0016-8. Epub 2018 Apr 30. Erratum in: Nat Med. 2018 Aug;24(8):1292. Erratum in: Nat Med. 2018 Aug;24(8):1290-1291. PMID: 29713087; PMCID: PMC6613387.

6. Schmitz R, Wright GW, Huang DW, Johnson CA, Phelan JD, Wang JQ et al. Genetics and Pathogenesis of Diffuse Large B-Cell Lymphoma. N Engl J Med. 2018 Apr 12;378(15):1396-1407. doi: 10.1056/NEJMoa1801445. PMID: 29641966; PMCID: PMC6010183.

7. Tripodo C, Zanardi F, Iannelli F, Mazzara S, Vegliante M, Morello G et al. A Spatially Resolved Dark- versus Light-Zone Microenvironment Signature Subdivides Germinal Center-Related Aggressive B Cell Lymphomas. iScience. 2020 Sep 16;23(10):101562. doi: 10.1016/j.isci.2020.101562. PMID: 33083730; PMCID: PMC7522121.

8. Ritchie ME, Phipson B, Wu D, Hu Y, Law CW, Shi W et al. Limma powers differential expression analyses for RNA-sequencing and microarray studies. Nucleic Acids Res. 2015 Apr 20;43(7):e47. doi: 10.1093/nar/gkv007. Epub 2015 Jan 20. PMID: 25605792; PMCID: PMC4402510.

9. Barrans SL, Crouch S, Care MA, Worrillow L, Smith A, Patmore R et al. Whole genome expression profiling based on paraffin embedded tissue can be used to classify diffuse large B-cell lymphoma and predict clinical outcome. Br J Haematol. 2012 Nov;159(4):441-53. doi: 10.1111/bjh.12045. Epub 2012 Sep 13. PMID: 22970711.

10. Sha C, Barrans S, Cucco F, Bentley MA, Care MA, Cummin T et al. Molecular High-Grade B-Cell Lymphoma: Defining a Poor-Risk Group That Requires Different Approaches to Therapy. J Clin Oncol. 2019 Jan 20;37(3):202-212. doi: 10.1200/JCO.18.01314. Epub 2018 Dec 3. Erratum in: J Clin Oncol. 2019 Apr 20;37(12):1035. PMID: 30523719; PMCID: PMC6338391.

11. Varano G, Raffel S, Sormani M, Zanardi F, Lonardi S, Zasada C et al. The B-cell receptor controls fitness of MYC-driven lymphoma cells via GSK3β inhibition. Nature. 2017 Jun 8;546(7657):302-306. doi: 10.1038/nature22353. Epub 2017 May 31. PMID: 28562582.

12. Tarte K, Zhan F, De Vos J, Klein B, Shaughnessy J Jr. Gene expression profiling of plasma cells and plasmablasts: toward a better understanding of the late stages of B-cell differentiation. Blood. 2003 Jul 15;102(2):592-600. doi: 10.1182/blood-2002-10-3161. Epub 2003 Mar 27. PMID: 12663452.

13. De Silva NS, Simonetti G, Heise N, Klein U. The diverse roles of IRF4 in late germinal center B-cell differentiation. Immunol Rev. 2012 May;247(1):73-92. doi: 10.1111/j.1600-065X.2012.01113.x. PMID: 22500833.

14. Sonja Boy, Marlene van Heerden, Roger Pool, Pascale Willem & Tomas Slavik. Plasmablastic lymphoma versus diffuse large B cell lymphoma with plasmablastic differentiation: proposal for a novel diagnostic scoring system. Journal of Hematopathology volume 8, pages 3–11 (2015). DOI 10.1007/s12308-014-0227-y.

15. O'Connor BP, Raman VS, Erickson LD, Cook WJ, Weaver LK, Ahonen C et al. BCMA is essential for the survival of long-lived bone marrow plasma cells. J Exp Med. 2004 Jan 5;199(1):91-8. doi: 10.1084/jem.20031330. PMID: 14707116; PMCID: PMC1887725.

16. Jourdan M, Caraux A, Caron G, Robert N, Fiol G, Rème T et al. Characterization of a transitional preplasmablast population in the process of human B cell to plasma cell differentiation. J Immunol. 2011 Oct 15;187(8):3931-41. doi: 10.4049/jimmunol.1101230. Epub 2011 Sep 14. PMID: 21918187.

17. Yoon SO, Zhang X, Lee IY, Spencer N, Vo P, Choi YS. CD9 is a novel marker for plasma cell precursors in human germinal centers. Biochem Biophys Res Commun. 2013 Feb 1;431(1):41-6. doi: 10.1016/j.bbrc.2012.12.102. Epub 2013 Jan 3. PMID: 23291167; PMCID: PMC3563937.

18. Won WJ, Kearney JF. CD9 is a unique marker for marginal zone B cells, B1 cells, and plasma cells in mice. J Immunol. 2002 Jun 1;168(11):5605-11. doi: 10.4049/jimmunol.168.11.5605. PMID: 12023357.

19. Xia Y, Xu-Monette ZY, Tzankov A, Li X, Manyam GC, Murty V et al. Loss of PRDM1/BLIMP-1 function contributes to poor prognosis of activated B-cell-like diffuse large B-cell lymphoma. Leukemia. 2017 Mar;31(3):625-636. doi: 10.1038/leu.2016.243. Epub 2016 Aug 29. PMID: 27568520; PMCID: PMC5837859.

20. Hans CP, Weisenburger DD, Greiner TC, Gascoyne RD, Delabie J, Ott G et al. Confirmation of the molecular classification of diffuse large B-cell lymphoma by immunohistochemistry using a tissue microarray. Blood. 2004 Jan 1;103(1):275-82. doi: 10.1182/blood-2003-05-1545. Epub 2003 Sep 22. PMID: 14504078.

21. Swerdlow, S.H.; Campo, E.; Harris, N.L.; Jaffe, E.S.; Pileri, S.A.; Stein, H. et al. WHO Classification of Tumours of Haematopoietic and Lymphoid Tissues, Revised 4th ed.; IARC: Lyon, France, 2017.

22. Hunter ZR, Xu L, Yang G, Tsakmaklis N, Vos JM, Liu X et al. Transcriptome sequencing reveals a profile that corresponds to genomic variants in Waldenström macroglobulinemia. Blood. 2016 Aug 11;128(6):827-38. doi: 10.1182/blood-2016-03-708263. Epub 2016 Jun 14. PMID: 27301862; PMCID: PMC4982454.

23. Maezawa Y, Nakajima H, Suzuki K, Tamachi T, Ikeda K, Inoue J et al. Involvement of TNF receptor-associated factor 6 in IL-25 receptor signaling. J Immunol. 2006 Jan 15;176(2):1013-8. doi: 10.4049/jimmunol.176.2.1013. PMID: 16393988.

24. Ahonen C, Manning E, Erickson LD, O'Connor B, Lind EF, Pullen SS et al. The CD40-TRAF6 axis controls affinity maturation and the generation of long-lived plasma cells. Nat Immunol. 2002 May;3(5):451-6. doi: 10.1038/ni792. Epub 2002 Apr 22. PMID: 11967542; PMCID: PMC2834483.

25. Green JA, Cyster JG. S1PR2 links germinal center confinement and growth regulation. Immunol Rev. 2012 May;247(1):36-51. doi: 10.1111/j.1600-065X.2012.01114.x. PMID: 22500830; PMCID: PMC3335345.

26. Myers RC, King RG, Carter RH, Justement LB. Lymphotoxin α1β2 expression on B cells is required for follicular dendritic cell activation during the germinal center response. Eur J Immunol. 2013 Feb;43(2):348-59. doi: 10.1002/eji.201242471. Epub 2012 Dec 5. PMID: 23112125; PMCID: PMC3753018.

27. Gars E, Butzmann A, Ohgami R, Balakrishna JP, O'Malley DP. The life and death of the germinal center. Ann Diagn Pathol. 2020 Feb;44:151421. doi: 10.1016/j.anndiagpath.2019.151421. Epub 2019 Nov 13. PMID: 31751845.

28. Wright GW, Huang DW, Phelan JD, Coulibaly ZA, Roulland S, Young RM et al. A Probabilistic Classification Tool for Genetic Subtypes of Diffuse Large B Cell Lymphoma with Therapeutic Implications. Cancer Cell. 2020 Apr 13;37(4):551-568.e14. doi: 10.1016/j.ccell.2020.03.015. PMID: 32289277.

29. Kotlov N, Bagaev A, Revuelta MV, Phillip JM, Cacciapuoti MT, Antysheva Z et al. Clinical and Biological Subtypes of B-cell Lymphoma Revealed by Microenvironmental Signatures. Cancer Discov. 2021 Jun;11(6):1468-1489. doi: 10.1158/2159-8290.CD-20-0839. Epub 2021 Feb 4. PMID: 33541860; PMCID: PMC8178179.

466 **FIGURE LEGENDS**

467 **Figure 1**
468 **A**, Digitalized slide selection of the Haematocylin and Eosin (H&E)-stained section of the
469 tonsil highlighting the presence of an aberrantly expanded germinal center (asterisk)
470 characterized by the presence of elements with plasmacytoid morphology (inset). On the H&E,
471 representative regions relative to germinal center dark zone (DZ) and light zone (LZ) areas,
472 peri-follicular (Peri) areas, and germinotropic plasmablastic expansion (GEx) areas, are
473 highlighted. Original magnification x50. **B**, Comparative analysis of H&E and IHC for Bcl-2,
474 Bcl-6, CD3, CD20, Kappa and Lambda light chain, Ki67, IRF4, IRF4/CD10, CD2, CD138 in
475 the DZ, LZ, Peri and GEx areas highlighted in A. **C,** Heatmap of the average expression of the
476 quantitative immunohistochemical analysis of the markers evaluated in the DZ, LZ, Peri, and
477 GEx areas highlighted in B.
478
479 **Figure 2**
480 **A,** Two-dimensional principal component reduction of the DZ (n=5), LZ (n=5), Peri (n=5), and
481 GEx (n=9) regions of interest (ROIs) profiles according to Digital Spatial Profiling of 1824
482 genes. **B**, Unsupervised hierarchical clustering of the 24 ROIs. **C**, Venn diagram of UP-
483 modulated genes from three different comparisons (i.e., GEx vs DZ, GEx vs LZ, and GEx vs
484 Peri). **D**, Venn diagram of DOWN modulated genes from three different comparisons (i.e.,
485 GEx vs DZ, GEx vs LZ, and GEx vs Peri). **E**, GEx signature genes. These genes are
486 significantly differentially expressed in GEx in each comparison. **F**, Heatmap of differentially
487 expressed genes in GEx as compared to DZ, LZ and Peri ROIs. The GEx signature shows a
488 high discriminatory capacity between GEx ROIs and the other regions.
489
490 **Figure 3**
491 **A,** Unsupervised clustering analysis of the 1147 DLBCL cases based on the GEx signature.
492 The signature identifies two distinct clusters; the blue one is characterized by a higher gene
493 expression, while a lower gene expression characterizes the green one. **B**, Survival analysis on
494 the two groups of DLBCL cases obtained from the unsupervised clustering. The overall
495 survival is significantly lower in the group characterized by the higher GEx signature
496 expression. The inset panel reports the cumulative distributions of the total GEx signature
497 expression per patient in the two groups (Kolmogorov-Smirnov p-value < 10e-10). **C**, Survival
498 analysis on the two groups – Q1 and Q4 - of DLBCL cases selected according to the cumulative
499 distribution of the total GEx signature. The first and the fourth quartiles identify the Q1 and Q4
500 groups, respectively. **D**, Survival analysis on the Q1 and Q4 groups of ABC-DLBCL cases. **E**,
501 Survival analysis on the Q1 and Q4 groups of GCB-DLBCL cases.
502

Figure 1

A

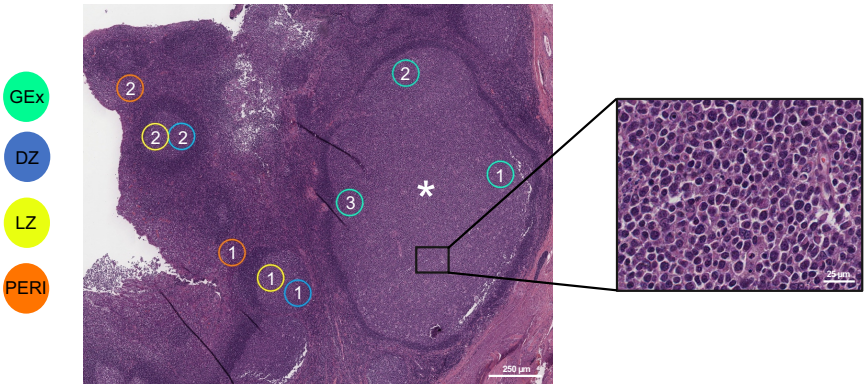

B

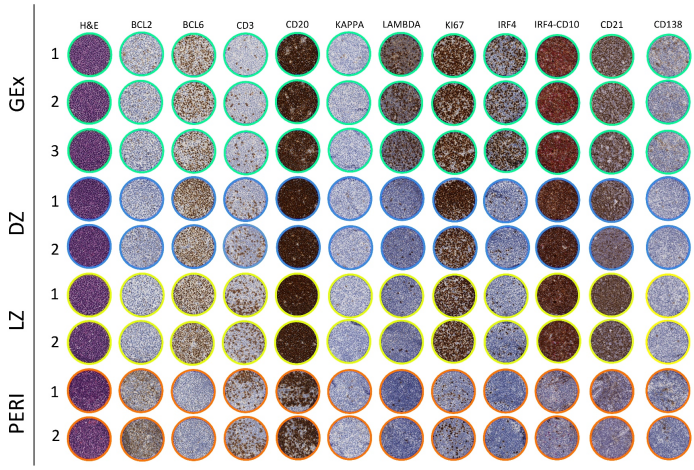

C

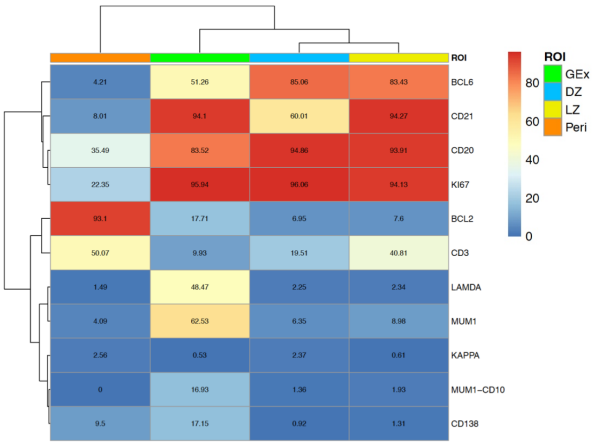

503

Figure 2

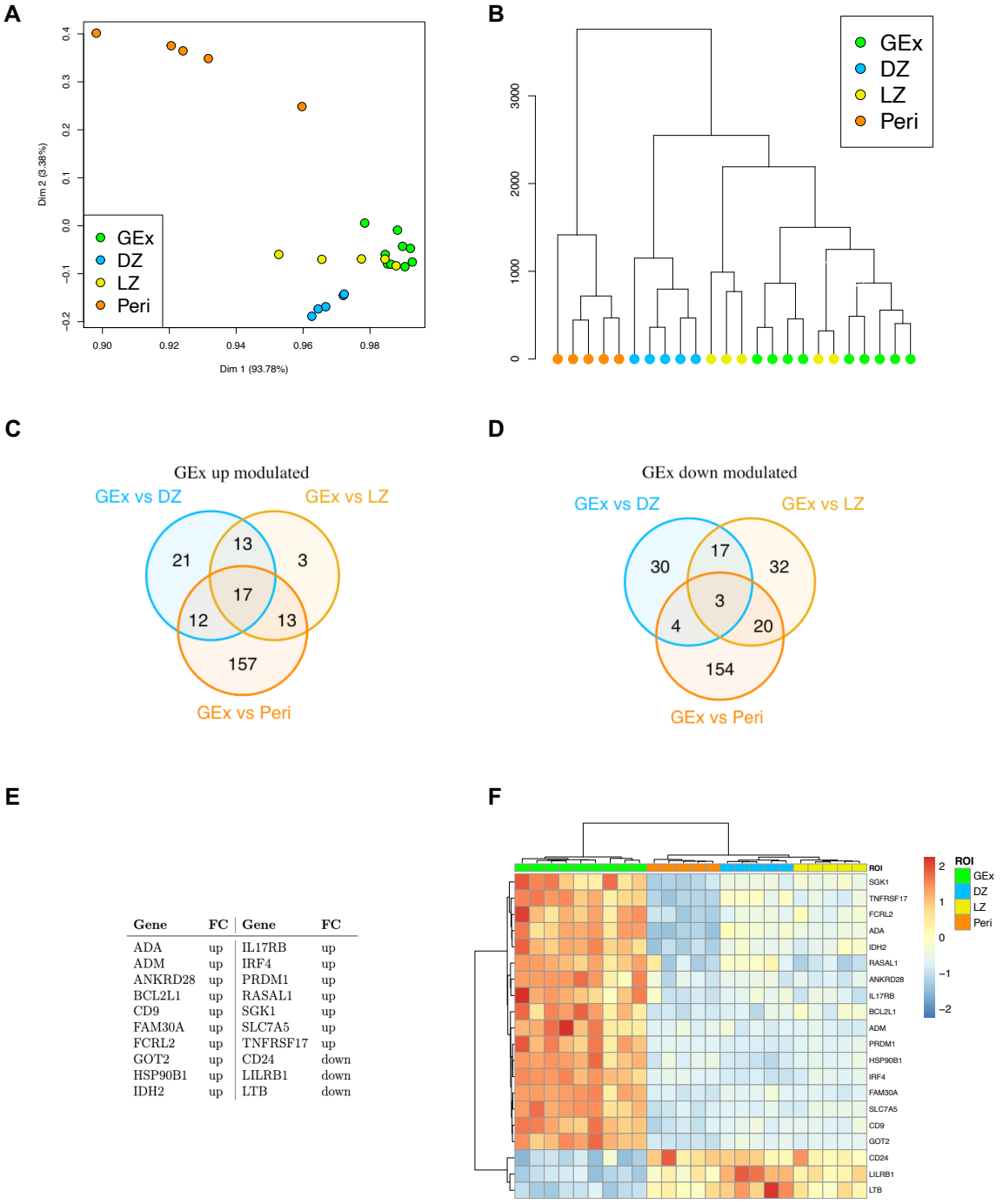

Gene	FC	Gene	FC
ADA	up	IL17RB	up
ADM	up	IRF4	up
ANKRD28	up	PRDM1	up
BCL2L1	up	RASAL1	up
CD9	up	SGK1	up
FAM30A	up	SLC7A5	up
FCRL2	up	TNFRSF17	up
GOT2	up	CD24	down
HSP90B1	up	LILRB1	down
IDH2	up	LTB	down

504

Figure 3

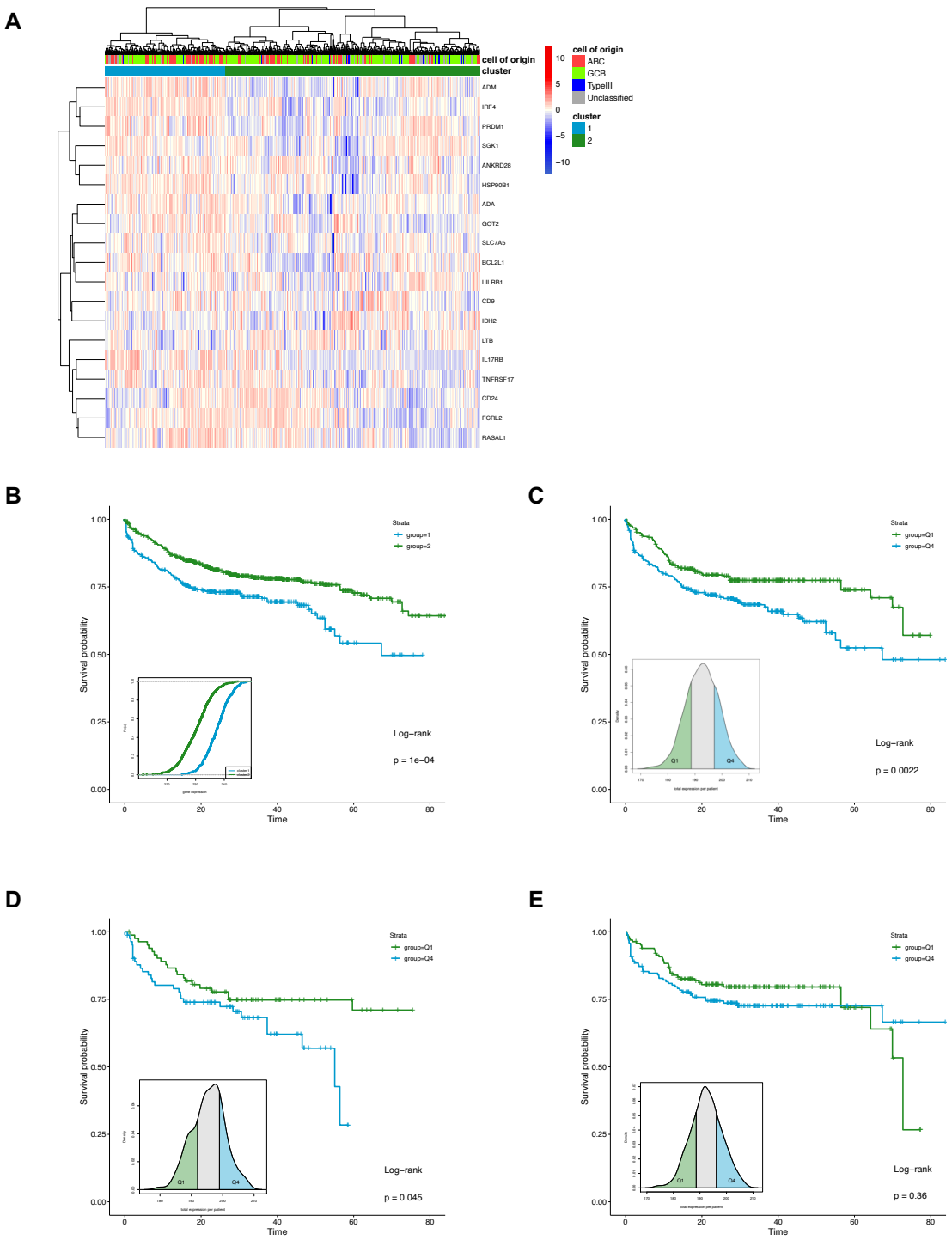
A
cell of origin
cluster
ADM
IRF4
PRDM1
SGK1
ANKRD28
HSP90B1
ADA
GOT2
SLC7A5
BCL2L1
LILRB1
CD9
IDH2
LTB
IL17RB
TNFRSF17
CD24
FCRL2
RASAL1
10
5
0
−5
−10
cell of origin
ABC
GCB
TypeIII
Unclassified
cluster
1
2
B
Survival probability
Time
Strata
group=1
group=2
Log−rank
p = 1e−04
C
Survival probability
Time
Strata
group=Q1
group=Q4
Log−rank
p = 0.0022
D
Survival probability
Time
Strata
group=Q1
group=Q4
Log−rank
p = 0.045
E
Survival probability
Time
Strata
group=Q1
group=Q4
Log−rank
p = 0.36

505